Probing the Contribution of Electronic Coupling to the Directionality of Electron Transfer in Photosynthetic Reaction Centers

Christine Kirmaier,[†] James A. Bautista,[‡] Philip D. Laible,[‡] Deborah K. Hanson,[‡] and Dewey Holten*,[†]

Department of Chemistry, Washington University, St. Louis, Missouri 63130, and Biosciences Division, Argonne National Laboratory, Argonne, Illinois 60439

Received: August 22, 2005; In Final Form: October 17, 2005

Subpicosecond transient absorption studies are reported for a set of *Rhodobacter* (*R.*) *capsulatus* bacterial photosynthetic reaction centers (RCs) designed to probe the origins of the unidirectionality of charge separation via one of two electron transport chains in the native pigment−protein complex. All of the RCs have been engineered to contain a heterodimeric primary electron donor (D) consisting of a bacteriochlorophyll (BChl) and a bacteriopheophytin (BPh). The BPh component of the M heterodimer (Mhd) or L heterodimer (Lhd) is introduced by substituting a Leu for His M200 or His L173, respectively. Previous work on primary charge separation in heterodimer mutants has not included the Lhd RC from *R. capsulatus*, which we report for the first time. The Lhd and Mhd RCs are used as controls against which we assess RCs that combine the heterodimer mutations with a second mutation (His substituted for Leu at M212) that results in replacement of the native L-side BPh acceptor with a BChl (β). The transient absorption spectra reveal clear evidence for charge separation to the normally inactive M-side BPh acceptor (H_M) in Lhd-β RCs to form $D^+H_M^-$ with a yield of ∼6%. This state also forms in Mhd-β RCs but with about one-quarter the yield. In both RCs, deactivation to the ground state is the predominant pathway of D* decay, as it is in the Mhd and Lhd single mutants. Analysis of the results indicates an upper limit of $V_L^2/V_M^2 \leq 4$ for the contribution of the electronic coupling elements to the relative rates of electron transfer to the L versus M sides of the wild-type RC. In comparison to the L/M rate ratio (k_L/k_M) ≈ 30 for wild-type RCs, our findings indicate that electronic factors contribute ∼35% at most to directionality with the other 65% deriving from energetic considerations, which includes differences in free energies, reorganization energies, and contributions of one- and two-step mechanisms on the two sides of the RC.

Introduction

The core of the bacterial photosynthetic reaction center (RC) consists of two polypeptides (L and M), both of which are folded into five membrane-spanning helices that house the bacteriochlorophyll (BChl), bacteriopheophytin (BPh), and quinone cofactors (denoted B, H, and Q, respectively) shown in Figure 1A.[1−4] Despite the pseudo-C_2 symmetry of the RC protein and cofactors, the complex is functionally asymmetric in that primary electron transfer is unidirectional to the L side (also referred to as the A side). In wild-type RCs, photoexcitation of the primary electron donor (P), a dimer of BChls, to its lowest excited singlet state (P*) initiates charge separation exclusively to the L side, forming $P^+H_L^-$ in ∼4 ps. Cofactor B_L assists in this initial phase of charge separation, with $P^+B_L^-$ serving parallel roles as a discrete intermediate in a "two-step" mechanism and as a virtual intermediate in a "one-step" (superexchange) mechanism (or in hybrid mechanisms). The current view of the free-energy ordering of the charge-separated states shown in Figure 2A supports a major role for the two-step mechanism by placing $P^+B_L^-$ 50−100 meV below P* and 150−200 meV above $P^+H_L^-$ in free energy. Subsequent $P^+H_L^- \rightarrow P^+Q_A^-$ electron transfer with $\Delta G = 0.5-0.6$ eV occurs with an ∼200-ps time constant, yielding $P^+Q_A^-$ with an overall quantum yield of ∼1.

The native unidirectional charge separation has been modulated via site-directed mutagenesis to produce RCs that undergo M-side electron transfer in yields as high as ∼35%.[5−15] (Charge-separated states on the M side of the RC have also been reported under conditions of high pulse energy or short wavelength excitation with native complexes.[16,17]) Studies on RCs in which charge separation to the M side is elicited by slowing electron transfer to the L side have given an estimate of ∼100 ps for the time constant for $P^* \rightarrow P^+H_M^-$ electron transfer in the wild-type RC.[5,6,8,10] This value, in comparison with 3−4 ps for $P^* \rightarrow P^+H_L^-$ transfer, is in accord with an ∼30-fold difference between the rates of charge separation to the L versus M sides of the RC postulated earlier.[18,19] On the normally inactive M side, subsequent $P^+H_M^- \rightarrow P^+Q_B^-$ electron transfer has also been demonstrated.[9,15,20−22] This process occurs with a time constant of a few nanoseconds, which is, yet again, an order of magnitude slower than $P^+H_L^- \rightarrow P^+Q_A^-$ electron transfer.[9,20]

The rate of an electron-transfer reaction is the product of a Franck−Condon factor, which is sensitive to the free energy change and reorganization energy for the process, and the electronic-coupling matrix element involving the initial and final states. The latter term reflects the orbital overlap between the donor and acceptor moieties and the electron-density distributions in the relevant excited and charge-separated states. For example, raising the free energy of $P^+B_L^-$ and lowering the free energy of $P^+B_M^-$ has been the key to promoting "wrong-

* Corresponding author. E-mail: holten@wuchem.wustl.edu.
[†] Washington University.
[‡] Argonne National Laboratory.

10.1021/jp054726z CCC: $30.25
Published on Web 11/22/2005

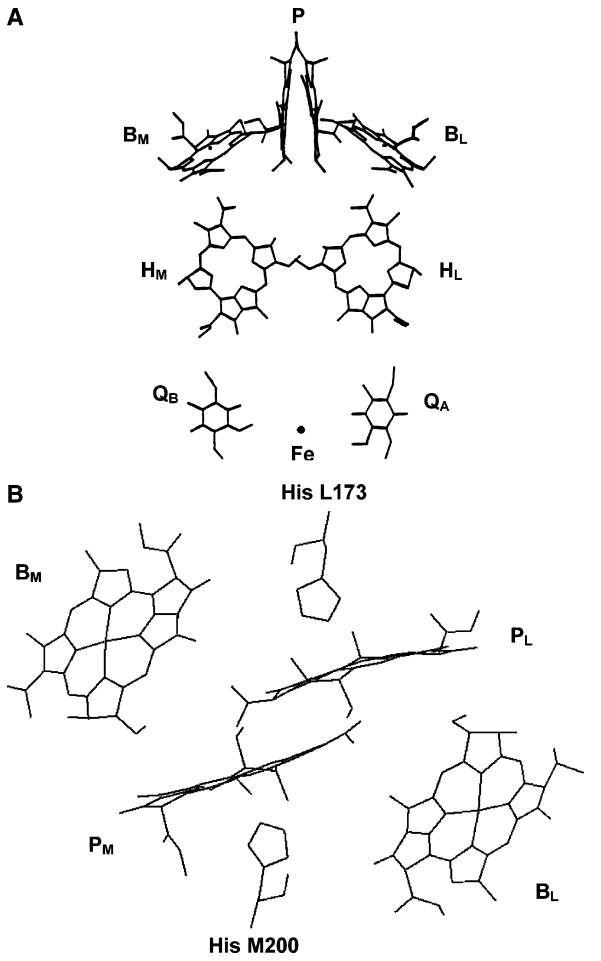

Figure 1. (A) Arrangement of the RC cofactors as determined by the X-ray structures of RCs from *Blastochloris viridis* and *R. sphaeroides*. (B) View roughly along the line of the C_2 symmetry axis of the RC, showing the four BChl cofactors in the wild-type structure and the His M200 and His L173 residues that are ligands to dimer P.

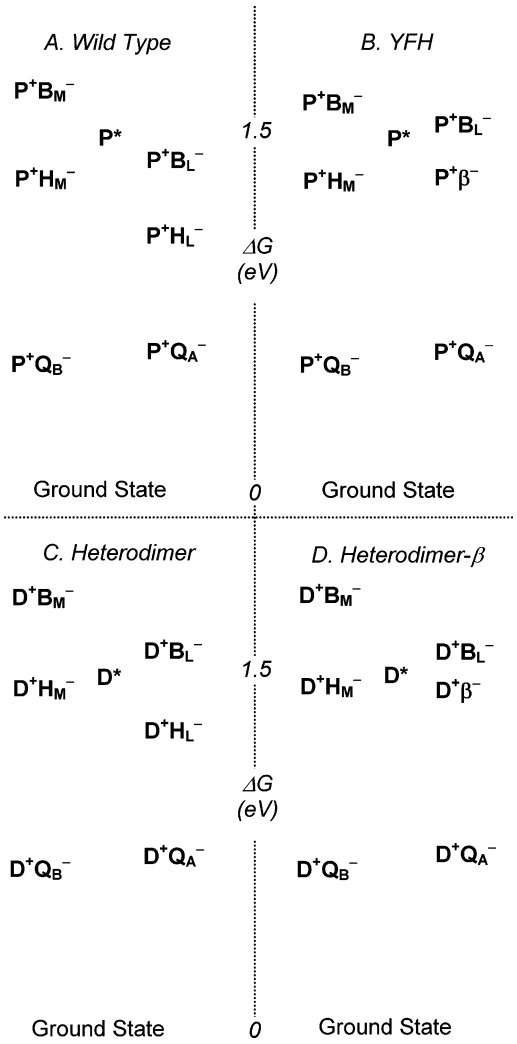

Figure 2. Schematic free-energy level diagrams for (A) wild-type, (B) YFH, (C) heterodimer, and (D) heterodimer-β RCs. P* is roughly 1.4 eV above the ground state. The positioning of the other states is not to scale but shows the key differences in the free-energy positions and ordering of the charge-separated states in the various RCs. See the text for further details.

way" electron transfer to give $P^+H_M^-$. This point is illustrated in the free energy diagram proposed for the YFH mutant (Figure 2B).[8] In these RCs, the native Phe L181 situated near P and B_M is changed to a Tyr, and the symmetry-related native Tyr M208 situated near P and B_L is changed to a Phe. Additionally, the native Leu M212 is changed to a His (the latter resulting in BChl (β) replacing H_L). Analysis of the results obtained for the YFH mutant led to the suggestion that the electronic couplings between P and the L- versus M-side cofactors contributes a factor of 2−7 to the overall ratio of ∼30 for the rates of electron transfer to the L versus M sides in the wild-type RC. The remaining factor of 15 to 4, respectively, would derive from energetic considerations, namely, the differences in the free energies and reorganization energies for formation of the charge-separated states on the L versus M sides. The principal contribution here is thought to be the relative free energies of $P^+B_L^-$ and $P^+B_M^-$ with respect to P* and thus the differing mechanisms for formation of $P^+H_L^-$ (two- and one-step mechanisms) versus $P^+H_M^-$ (one-step mechanism only) in the native RC. In other words, these results, and those obtained from other studies,[6,11,23,24] suggest that the contribution of electronic matrix elements is at most comparable to the role of energetics, but could be far less important. Several theoretical studies have suggested a much larger, even preponderant, role of an asymmetry in electronic matrix elements in the unidirectionality of electron transfer.[25−30]

To advance our understanding of the balance between these two factors further, it would be useful to modulate in a controlled way the electronic coupling matrix elements on the L and M sides, in parallel to studies in which the free energies of the states have been modulated. This is a difficult challenge. There is no rational way to change the spatial orbital overlaps involving P, B_L, and H_L versus those involving P, B_M, and H_M. However, there are opportunities to alter the electron-density distributions in the relevant donor and acceptor states, namely, P*, $P^+B_L^-$, $P^+B_M^-$, $P^+H_L^-$, and $P^+H_M^-$. In considering the orbital characteristics of the primary donor, we will call the two halves of the native dimer P_L and P_M, with the L and M subscripts referring to the respective polypeptide that provides the His ligand to the central Mg^{2+} ion of the respective BChl component, namely, His L173 and His M200 (using *R. capsulatus* numbering). Figure 1B shows a view along the C_2 axis of the RC of P, its His ligands, and monomer BChls B_L and B_M.

In bacterial RCs, the electron-density distributions in P* and P^+ are asymmetric because of environmental differences of the two constituent BChls. One source is local and global differences in the dielectric environment experienced by P_L and P_M (Figure 1B). In terms of specific interactions, P_L has a hydrogen bond (from His L168) to the acetyl group of ring I, whereas P_M does

not. ENDOR and ESR experiments have shown that the hole in P^+ visits both halves of the dimer but is not shared equally.[31,32] For P*, electronic asymmetry derives from the relative contributions (mixing) of the locally excited configurations $P_L{}^*P_M$ and $P_LP_M{}^*$ (linear combinations of which are the exciton configurations) and the charge-transfer (CT) configurations $P_L{}^+P_M{}^-$ and $P_L{}^-P_M{}^+$ (linear combinations of which are the charge-resonance configurations), with the energies of the latter being particularly sensitive to the dielectric environment. The degree of net CT character of P* (derived from the difference in the contributions of $P_L{}^+P_M{}^-$ and $P_L{}^-P_M{}^+$) has been invoked in describing the ground-state absorption band of P,[25,33−39] hole-burning and Stark spectra,[38,40−45] properties of the triplet state of the dimer,[46−49] and the directionality and mechanism of initial charge separation.[25,28,35,50−52] Both calculations and experiments have suggested that the protein asymmetry imparts a small net $P_L{}^+P_M{}^-$ CT character to P* in the wild-type RC.[24,25,27,28,39,53,54]

Among the earliest studied site-directed mutant RCs were those in which the two His ligands to the central Mg of the BChl components of P are changed individually to the non-coordinating residue, Leu.[55,56] The primary electron donor in these RCs is a heterodimer (denoted D) composed of a BChl and a BPh, the pigment change to BPh being the result of the loss of the His ligand to the central Mg^{2+} ion of that BChl macrocycle. Heterodimer RCs are extreme examples of modulating the inherent electronic asymmetry of the primary donor owing to the difference in the redox potentials of BChl and BPh. In solution, BPh is 150−300 meV easier to reduce (and harder to oxidize) than BChl.[57] This redox differential within D and the results of picosecond transient absorption studies led to the original suggestion that D* is endowed with significant net CT character.[56,58−63] Stark, EPR, and resonance Raman measurements have also shown that D* in heterodimer RCs has much more CT character than P* in wild-type RCs, that D^+ has a more asymmetric charge distribution than P^+ with the hole preferentially localized on the BChl moiety,[64−70] and that these effects can be modulated by hydrogen-bonding interactions.[53,71]

The heterodimer RCs are good vehicles for studying the effects of electronic asymmetry on unidirectional electron transfer. For the *R. capsulatus* heterodimer mutant in which His residue M200 is changed to Leu (denoted the Mhd mutant), the $D(BChl)_L{}^+D(BPh)_M{}^-$ CT configuration is greatly stabilized compared to $D(BChl)_L{}^-D(BPh)_M{}^+$. Indeed, it is believed that $D(BChl)_L{}^+D(BPh)_M{}^-$ is even lower in energy than the locally excited configurations $D(BChl)_L{}^*D(BPh)_M$ and $D(BChl)_LD(BPh)_M{}^*$ and thus makes the predominant contribution to the electronic nature of D*.[59,63,72] Similarly, for the heterodimer mutant in which His residue L173 is changed to a Leu (the Lhd mutant), the $D(BPh)_L{}^-D(BChl)_M{}^+$ CT configuration is greatly stabilized compared to $D(BPh)_L{}^+D(BChl)_M{}^-$ and dominates the nature of D*. Despite this anticipated gross reversal of the biasing of the charge distribution in D* in the Mhd and Lhd mutants, picosecond transient absorption studies have not revealed clear evidence for electron transfer to H_M in either mutant.[56,58−63]

In addition to distorting significantly the charge distribution in D* and D^+, the heterodimer mutations influence the free energies of the states involved in charge separation, as is shown in Figure 2C. First, D* is slightly lower in energy than P*. More significantly, the oxidation potential of D is ∼160 meV more positive than the value of +500 meV for P (+658 meV for the Mhd and +676 meV for the Lhd in *R. sphaeroides*).[63,71,73] Because of the difference in the D/D^+ versus P/P^+ potentials, all of the charge-separated states are at a higher free energy in the heterodimer mutants than in wild-type (Figure 2C). A significant consequence of these two changes is that $D^+B_L{}^-$ is almost certainly higher in free energy than D*, likely by at least 50 meV, and therefore cannot serve as an intermediate in a two-step mechanism of electron transfer to H_L as it does in the wild type. Not surprisingly, $D^* \rightarrow D^+H_L{}^-$ electron transfer is more than 10 times slower than $P^* \rightarrow P^+H_L{}^-$ electron transfer (∼40 ps in Mhd vs 3−4 ps in wild type).[56,60] Thus, electron transfer to both the L and M sides in heterodimer RCs should occur solely by the one-step superexchange mechanism, albeit with different rate constants because of differences in superexchange energy denominators involving $D^+B_L{}^-$ or $D^+B_M{}^-$ as virtual intermediates.

Because the increased oxidation potential of D will increase the free energies of the charge-separated states by the same amount, $D^+H_L{}^-$ is expected still to be lower than $D^+H_M{}^-$ by the same gap that separates $P^+H_L{}^-$ and $P^+H_M{}^-$ in the wild-type RC. In the present study, we have replaced the BPh cofactor H_L with BChl (denoted β) in the Mhd and Lhd mutants of *R. capsulatus* by substituting a His for the native Leu at M212, resulting in the Mhd-β and Ldh-β RCs. The free energies of $P^+\beta^-$ and $P^+H_M{}^-$, on the L and M sides of the RC, respectively, should be more equal owing, again, to the fact that BChl is harder to reduce than BPh. Thus, $D^+\beta^-$ is higher in free energy than $D^+H_L{}^-$ and more comparable to the (presumed) free energy of $D^+H_M{}^-$ (Figure 2D). The Mhd-β and Lhd-β RCs thus provide a significant step toward equalizing the free-energy contributions to the rates of electron transfer to the two branches, in addition to electron transfer occurring by the same (superexchange) mechanism to the two sides. Because they contain one less BPh pigment compared to the single heterodimer mutants, the heterodimer-β combinations also alleviate some of the spectral congestion and difficulty of probing electron transfer to H_M via bleaching of its Q_X band at 528 nm. These combined properties make the heterodimer-β RCs a new platform for assessing the relative balance between the contributions of free energy and electronic coupling to the rates of electron transfer to the L versus M sides of the RC.

Experimental Section

Mutant Construction. Site-directed mutagenesis was carried out using the QuikChange kit (Stratagene) with L- or M-gene templates that were cloned in pBS^- (Stratagene). Primers substituting a leucine residue (CTA) for the native histidine at M200 resulted in the creation of an *Sty*I restriction enzyme site that was used for screening candidate mutants. The same set of primers was employed to generate the H(M200)L−L(M212)H double mutant from the M-gene template carrying the L(M212)H substitution described previously.[5] Similarly, leucine (CTC) was substituted for histidine at L173 using primers that also led to the loss of an *Nsp*I site. Mutations were verified by DNA sequencing. As described previously,[74] mutant L and M genes were swapped with their wild-type counterparts in plasmid pUHTMluBgl:α^- for expression in *R. capsulatus*. Strains harboring this plasmid express RCs in an antennaless background; the RCs carry a C-terminal heptahistidine tag on the M subunit that facilitates their purification by immobilized metal affinity chromatography (IMAC). Procedures for conjugal transfer of expression plasmids to *R. capsulatus* host strain U43 (LHI^- $LHII^-$ RC^-)[55] followed by selection and purification of transconjugants have been described.[74] Strains were propagated routinely under chemoheterotrophic conditions published previously.[74]

Semiautomated RC Purification. The photosynthetic membranes of strains expressing mutant RCs lack both the LHI and LHII antennae complexes. As was shown previously,[75] these strains allow for solubilization of RCs in milder conditions (without loss of yield) and, thus, facilitate purification of mutant RCs that are too fragile to withstand traditional protocols. In this study, solubilization of membrane proteins proceeded in the presence of 1% LDAO at room temperature with membrane debris removed thereafter by ultracentrifugation at 240 000 × *g* for 1.5 h. All of the chromatographic procedures were performed in semiautomated fashion using a fast-protein-liquid-chromatography system (ÄKTA-FPLC, GE Healthcare, Uppsala, Sweden) that has been highly modified to accommodate the needs of membrane protein purification. The hardware and in-house scripts used to purify membrane proteins and membrane protein complexes from relatively large volumes of detergent-solubilized extracts have been described previously.[76] The only change made to accommodate purification of mutant *R. capsulatus* RC complexes was the use of larger sample vessels to accommodate extracts whose starting volumes could approach 1 L. Purified fractions were collected following elution from a buffer exchange column in a solution containing 10 mM Tris-Cl (pH 8.0) and 0.05% LDAO. RCs were concentrated centrifugally (Amicon Ultra; 100 kDa cutoff), frozen in liquid N_2, and stored at −80 C until use.

Spectroscopy. The time-resolved absorption measurements were carried out on an apparatus that utilizes ∼130-fs excitation and white-light probe flashes. Samples (2.5−3 mL of RCs) were held in an ice-cooled reservoir and flowed through a 2-mm-path-length cell. This arrangement maintained a sample temperature of ∼10 °C. For both of the experiments that probed through the near-infrared region (820−1000 nm) and those that probed the 500−700 nm region, the heterodimer-containing RCs had a ground-state absorption at ∼850 nm of ∼0.5 and at ∼800 nm of ∼3.0, in a 2-mm-path-length cell. For all experiments, the RCs were suspended in 10 mM Tris, pH 7.8/0.05% LDAO. Further details of the instrumentation and data analysis procedures can be found elsewhere.[77,78]

Results

RC Purification. The supply of mutant RC samples for the time-resolved experiments, especially those that were produced in *R. capsulatus* cells in low yield, was advanced tremendously by the availability and implementation of technology for their purification by semiautomated methods.[76] The use of the ÄKTA-FPLC for affinity chromatography had marked effects on the efficiency and reproducibility of RC purification. In regards to efficiency, the FPLC worked without human intervention (usually overnight) in purifying polyhistidine-tagged RCs from solubilized membrane extracts [in some cases, large volumes (up to 1 L) of membrane extracts] in about an 8-hour period. This compares to previous protocols for purification of heterodimer mutant RCs that used traditional fractionation steps and ion-exchange chromatographies that took several days.[55,79] It is likely that the implementation of automation led to the first reported success in the purification of the *R. capsulatus* Lhd mutant RC in yields high enough for use in pump−probe spectroscopic experiments; the study of the Lhd-β RC definitely could not have been conducted in its absence. The fact that RC isolation can now proceed from cells on one morning to the point of concentrated and frozen RCs by noon the next day will go a long way to make the study of highly mutated RCs more routine. It might also allow groups to revisit "finicky" mutant RCs that were detected clearly in native membranes but failed the purification process.

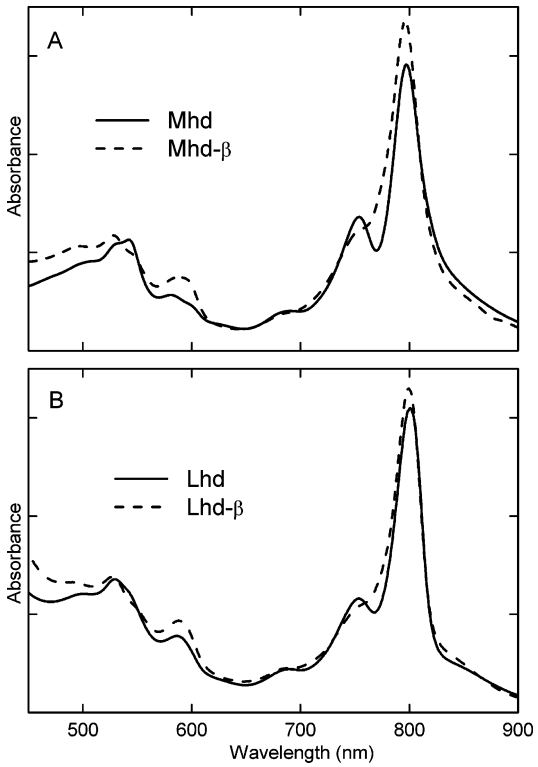

Figure 3. Ground-state absorption spectra of (A) Mhd and Mhd-β RCs and (B) Lhd and Lhd-β RCs at 295 K.

In regards to reproducibility, the lack of variation between purification "runs" (purity ratios and yields for a given amount of starting material) gave us the confidence to pool fractions repeatedly from replicate cell cultures and purification routines, knowing that the resultant RCs would resemble, with remarkable consistency, those purified previously. As much as 50 L of cell culture were required for some of the mutant strains described in this study because the amounts of RCs expressed on a per cell basis that could be purified in functional form decreased rapidly in the order of WT, Mhd, Mhd-β, Lhd, and Lhd-β. We attempted to start each purification run with a specific amount of RCs by monitoring the 800-nm absorption level, but the yields of Lhd and Lhd-β RCs were so low that the membrane/detergent slurry was too thick; thus, solubilization was not quantitative. Although "normal" purifications commenced with solubilized slurries of ∼300 mL, the process for the Lhd and Lhd-β RCs used volumes up to 900 mL. Even though the process was scaled up to this level, multiple runs were needed to obtain sufficient quantities of Lhd-β RCs.

Ground-State Spectra and Pigment Content. The ground-state absorption spectra of RCs from the Mhd and Lhd mutants are shown in Figure 3. They are similar to the spectra of Mhd and Lhd RCs from *R. sphaeroides* and the Mhd RC from *R. capsulatus* reported previously.[55,56,60,72] The spectrum of the *R. capsulatus* Lhd mutant is reported here for the first time. The absorption spectrum of RCs containing a BChl-BPh heterodimer is distinguished from that of RCs containing the wild-type BChl-BChl dimer in particular by the lower oscillator strength and broad, nearly featureless contour of the long-wavelength absorption of D, which extends past 900 nm. Compared to the spectrum of wild-type RCs (not shown), in the visible region the absorption band near 600 nm is smaller and there is increased absorption in the 540−550 nm region. Qualitatively, these changes are consistent with loss of a BChl-like Q_X absorption (590−600 nm region) and gain of a BPh-like Q_X absorption (540−550 nm). Heterodimer RCs from both *R. capsulatus* and

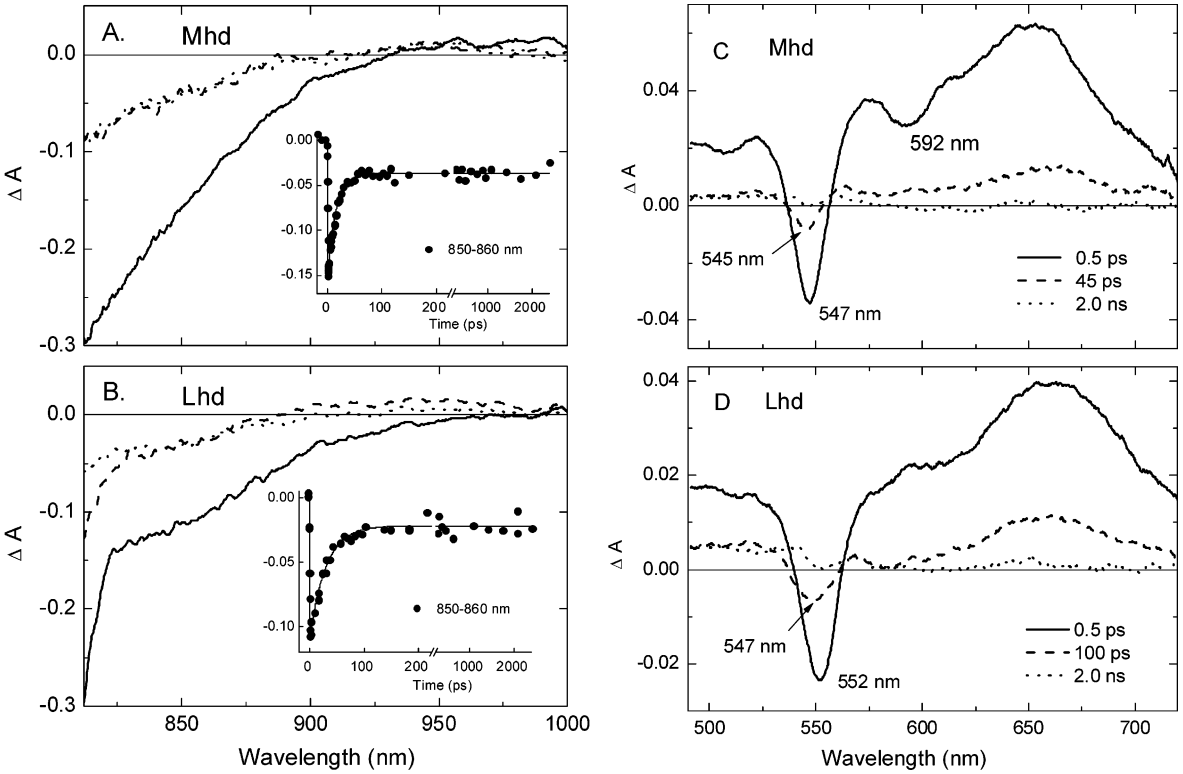

Figure 4. Panels A and B show transient absorption difference spectra acquired following a 130-fs 590-nm excitation flash for the Mhd and Lhd mutants, respectively. Parts C and D show similar spectra in the visible region, acquired following a 130-fs 850-nm excitation flash. The solid, dashed, and dotted spectra for the Mhd RCs in part A were acquired at the times shown in part C. Similarly, the solid, dashed, and dotted spectra for the Lhd RCs in part B were acquired at the times shown in part D. The insets in parts A and B show the time course of ΔA data averaged between 850 and 860 nm (circles) and a fit to the instrument function plus one exponential plus a constant (solid line) for the Mhd and Ldh RCs, respectively.

R. sphaeroides have been shown by pigment extraction and/or metals analysis to contain the expected three BChls and three BPhs,[56,60,71] and later crystal structures confirmed the presence of a BChl−BPh heterodimer with the loss of the Mg that no longer had its coordinating His ligand to one side of the primary electron donor (D).[80,81]

As has been shown to occur in all previous mutants in which the native Leu at M212 is replaced with a His residue (see, e.g., refs 5 and 82), we expect that combining the Mhd and Lhd mutants each with this mutation will yield RCs that contain β in place of H_L. The heterodimer-β mutant RCs are thus expected to contain four BChls and two BPhs as do wild-type RCs, but with two swaps of the BChl and BPh cofactors. The ground-state absorption spectra of RCs from the Mhd-β and Lhd-β mutants shown in Figure 3 are consistent with this change in pigment content. Qualitatively, the differences in the spectra for the heterodimer-β mutants compared to the heterodimer mutants include loss of the 545-nm Q_X and 760-nm Q_Y absorption bands of H_L and gain of BChl absorption (due to β) in the Q_X (590−600 nm) and Q_Y (800 nm) regions. On the basis of these spectra, all previous work on RCs containing a His residue at M212, and the results presented below, we are confident that the Mhd-β and Lhd-β RCs contain a BChl-BPh heterodimer and a BChl (β) in place of the native L-side BPh (H_L).

Primary Electron-Transfer Reactions of the L and M Heterodimers. Transient absorption spectra in the near-infrared and visible regions and representative kinetic data are shown in Figures 4 and 5 for Mhd and Lhd RCs. The data are similar to those reported previously for Mhd RCs from *R. capsulatus* and for the Mhd and Lhd mutants from *R. sphaeroides*. Excitation of either heterodimer produces D* and results in bleaching of the near-infrared absorption of D (0.5-ps spectra of Figure 4A and B). For Mhd RCs, there is concomitant bleaching near 547 and 592 nm (near the positions of the Q_X absorption bands of BPh and BChl, respectively) and a broad absorption band with a peak at 650 nm (Figure 4C) that is analogous to the 665-nm anion band of H_L^- observed in the transient spectrum of $P^+H_L^-$ in wild-type RCs. This 650-nm absorption band in the D* spectrum was the basis originally for the assignment that D* has significant $D(BChl)_L^+D(BPh)_M^-$ CT character.[56,58,59] The visible-region spectrum for the Lhd mutant is similar but red-shifted, with a BPh-like bleaching at 552 nm and the broad anion-band absorption near 660 nm (Figure 4D). Interestingly, there is no distinct BChl-type Q_X bleaching between 580 and 600 nm in the Lhd D* spectrum that would parallel the 592-nm D* bleaching in the Mhd spectrum.

The D* lifetimes for the Mhd and Lhd mutants are 14 ± 4 ps and 25 ± 5 ps, respectively; representative kinetic data and fits to the decay of D bleaching are shown in the insets to Figure 4A and B. The 14-ps time constant for D* decay found here for the Mhd RC reproduces the value reported previously for this *R. capsulatus* mutant.[56] Immediately following D* decay (dashed spectra in Figure 4A and B), most of the near-infrared D bleaching has decayed for both Mhd and Lhd RCs. We take this as reflecting recovery of the ground state; that is, the data contain little or no contribution from stimulated emission from D*. The absence of D* stimulated emission in this spectral region has been discussed previously for heterodimer RCs at room temperature[59,61] and is particularly relevant to the blue side of the ground-state absorption of D (e.g., 830−870 nm).[83] Thus, we assign the ~75% decay of bleaching that is seen in Figure 4 for the Mhd RC and ~70% for the Lhd RC to reflect decay of D* to the ground state.[84]

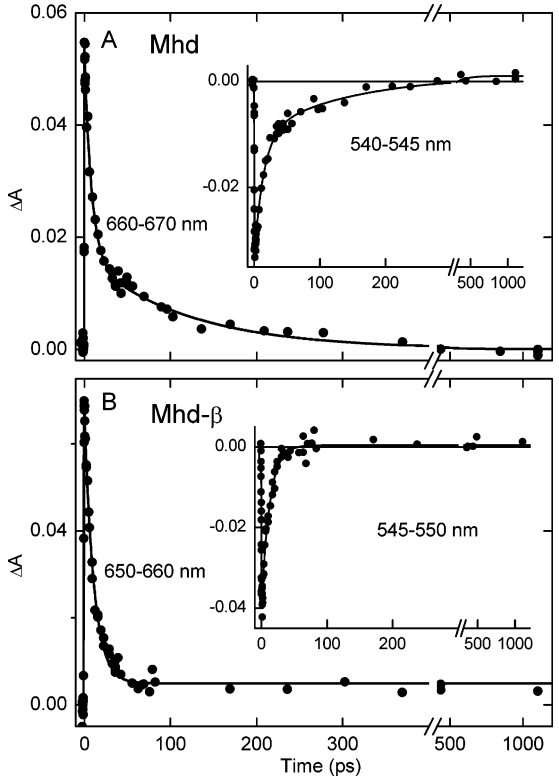

Figure 5. Kinetic data acquired using 130-fs excitation flashes at 850 nm for Mhd and Mhd-β RCs. Part A shows the ΔA data (circles) averaged between 660 and 670 nm (main part of figure) and between 540 and 545 nm (inset) for the Mhd mutant and a fits to the instrument response plus two exponentials plus a constant (solid lines). Panel B shows analogous data for the Mhd-β mutant and fits to the instrument response plus one exponential plus a constant.

In both mutants, the remaining 25−30% of the initial population of D* undergoes charge separation to give $D^+H_L^-$, as is indicated by the spectra and kinetics in the visible region (Figure 4C and D). For Mhd RCs, the spectrum observed at 45 ps has an anion-band feature that is red-shifted from the 650-nm position of D* to 665 nm, which is the known position of the absorption band of H_L^-. The Q_X bleaching at 45 ps in the Mhd RC sample is slightly blue-shifted (545 nm) compared to that seen in the D* spectrum (547 nm). This also is consistent with electron transfer to H_L; formation of $D^+H_L^-$ would result in combination bleaching of the 547-nm band of D and bleaching of the (known) 542-nm Q_X band of H_L. Qualitatively, the overall reduced amplitude of bleaching at 45 ps compared to that in the D* spectrum at 0.5 ps is consistent with the majority (75%) decay of D* to the ground state and the 25% yield of an electron-transfer product (e.g., $D^+H_L^-$) calculated from the 830−870 nm D bleaching data for the Mhd RC. A fit of the kinetic data between 540 and 560 nm (the Q_X bleaching) and throughout the anion absorption region (600−700 nm) to two exponentials plus a constant yields time constants of 12 ± 3 ps and 110 ± 10 ps (Figure 5A). The first time constant reflects the D* lifetime and agrees with that found in the near-infrared region. We associate the 110-ps time constant with the $D^+H_L^-$ lifetime, which reflects predominantly $D^+H_L^- \rightarrow D^+Q_A^-$ electron transfer. (There is little evidence that $D^+H_L^- \rightarrow$ ground state (recovery) takes place. Although we cannot rule out a few percent yield of this process, we will not consider it further here.) This 110-ps time constant is the same as that found previously for $D^+H_L^- \rightarrow D^+Q_A^-$ electron transfer in the Mhd *R. capsulatus* RC and is similar to the 180-ps time constant for $P^+H_L^- \rightarrow P^+Q_A^-$ electron transfer in wild-type RCs.

Analysis of the data obtained in the visible and anion regions for the Lhd RC parallels that described above for the Mhd RC. Following D* decay, the spectrum acquired at 100 ps is again consistent with formation of $D^+H_L^-$, as reported previously for this mutant of *R. sphaeroides*.[60] The Q_X bleaching is again blue-shifted compared to the D* spectrum at 0.5 ps (Figure 4D). This blue shift is somewhat larger in the Lhd mutant given the initial position of D* Q_X bleaching in the Lhd mutant at 552 nm (versus 547 nm for the Mhd RC). However, the H_L anion band of $D^+H_L^-$ at 665 nm in the Lhd spectrum is less distinct from the 660-nm anion band of D*. A fit of the kinetic data in the Q_X bleaching (540−560 nm) and throughout the 600−700 nm region to two exponentials plus a constant gives time constants of 20 ± 6 ps and 215 ± 30 ps (data not shown). Again these are associated with, respectively, the D* lifetime and the $D^+H_L^-$ lifetime, the latter, again, predominantly reflecting $D^+H_L^- \rightarrow D^+Q_A^-$ electron transfer. The 215-ps time constant for $D^+H_L^- \rightarrow D^+Q_A^-$ electron transfer in the Lhd mutant is about a factor of 2 longer than that found for the Mhd mutant. The same trend was found previously for Mhd and Lhd RCs from *R. sphaeroides*, where the time constants for $D^+H_L^- \rightarrow D^+Q_A^-$ electron transfer are 150 and 250 ps, respectively.[60] The longer D* lifetime that we find here for the Lhd compared to the Mhd (25 ps vs 14 ps) also parallels the 42 ps and 18 ps D* lifetimes in the *R. sphaeroides* Lhd and Mhd mutants, respectively.[60]

In summary, results for the Mhd mutant are essentially the same as those found in the original work on this heterodimer RC, and the new results on the Lhd mutant RC mirror trends found previously for the analogous Mhd and Lhd mutant RCs of *R. sphaeroides*. A main new result, discussed in greater detail below, is that there is no clear evidence for electron transfer to H_M in either of these two heterodimer RCs, as determined by an absence of discernible bleaching of the Q_X band of H_M at 528 nm. This conclusion was reported in the original studies of heterodimer RCs; however, the signal-to-noise of the current experiments is far superior, so the point is worth confirming. Additionally, these results on the Mhd and Lhd RCs provide controls for the heterodimer-β combination mutants investigated under the same conditions and are described next.

Primary Electron-Transfer Reactions of Mhd-β and Lhd-β RCs. Figure 6 parallels Figure 4 in presenting data for Mhd-β and Lhd-β RCs. It is immediately clear from the magnitude of bleaching of D as a function of time (panels A and B), that the yield of D* → ground state is ≥85% for both mutants. For both the Mhd-β and Lhd-β RCs, the decay of bleaching between 830 and 870 nm can be fit by a single-exponential plus a constant, with resulting D* lifetimes of 15 ± 4 and 40 ± 8 ps, respectively. Representative data and fits are shown in the inserts to Figure 6A and B. The fits give a long-time yield (asymptote) of D bleaching on the order of 5−10% for Mhd-β RCs and 10−15% for Lhd-β RCs, as reflected in the spectra taken at 50 ps (Mhd-β) and 135 ps (Lhd-β). Thus, there is an even lower yield of charge-separation from D* in the heterodimer-β RCs than in the heterodimer single mutants.

In the Q_X and anion regions, the 0.5-ps D* spectrum for Mhd-β RCs (Figure 6C) is the same within experimental error as that for Mhd RCs (Figure 4C). The same is true for the D* spectrum of Lhd-β RCs (Figure 6D) and Lhd RCs (Figure 4D). The spectra acquired at longer times confirm a lower overall yield of charge separation in the two β-containing RCs compared to the heterodimer single mutants. The spectrum acquired at 50 ps has a much smaller Q_X bleaching for Mhd-β versus that

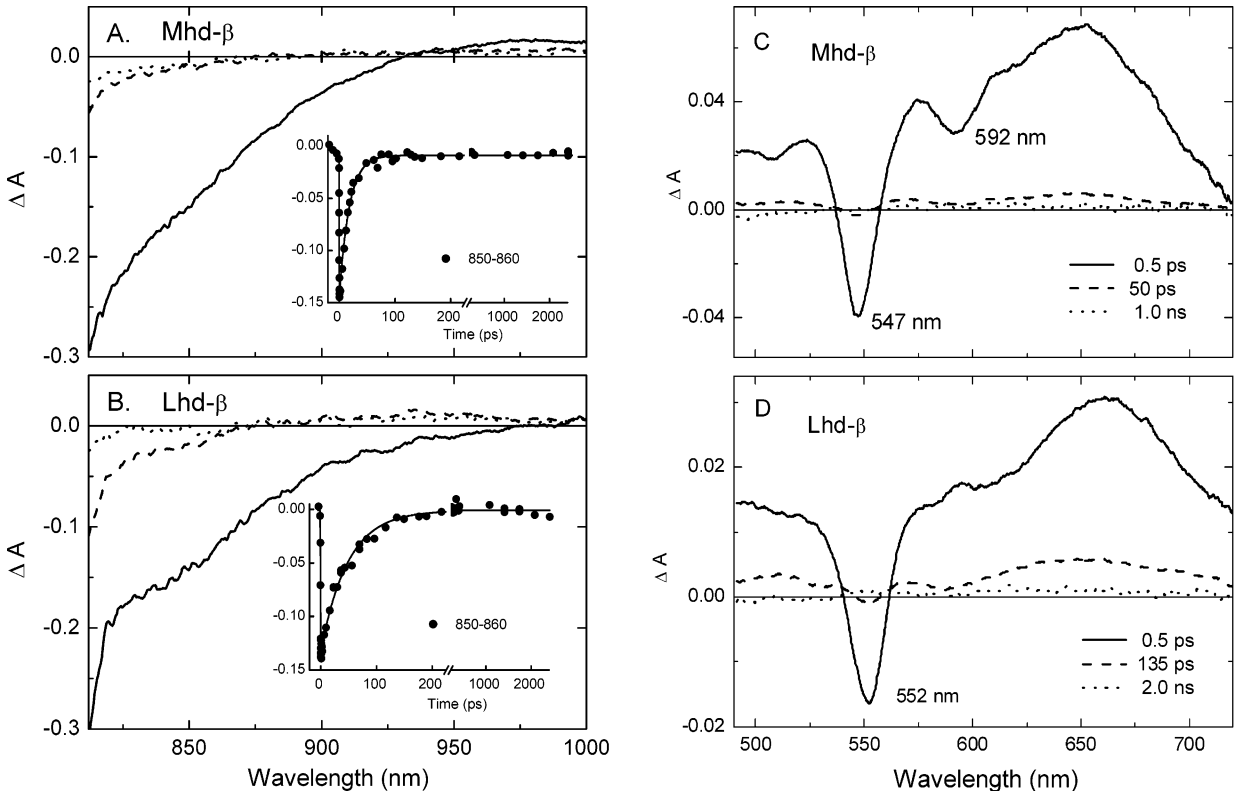

Figure 6. Panels A and B show transient absorption difference spectra acquired following a 130-fs 590-nm excitation flash for the Mhd-β and Lhd-β mutants, respectively. Parts C and D show similar spectra in the visible region, acquired following a 130-fs 850-nm excitation flash. The solid, dashed, and dotted spectra for the Mhd-β RCs in part A were acquired at the times shown in part C. Similarly, the solid, dashed, and dotted spectra for the Lhd-β RCs in part B were acquired at the times shown in part D. The insets to parts A and B show the time course of the ΔA data averaged between 850 and 860 nm (circles) and a fit to the instrument function plus one exponential plus a constant (solid line) for the Mhd-β and Ldh-β RCs, respectively.

seen in the 45-ps spectrum of Mhd RCs, and much smaller amplitude of anion absorption in the 600−700 nm region. In parallel, Figure 5A for Mhd RCs shows decay components for both D* and a charge-separated state, whereas the latter is not resolved in Figure 5B for Mhd-β RCs. A detailed comparison of the magnitudes of these absorption changes indicates an ∼7% yield of charge-separated product(s) formed from D* in Mhd-β RCs. Similar comparison of the spectra at 135 and 100 ps for Lhd-β and Lhd RCs, respectively, gives an ∼15% yield of charge-separated product(s) from D* in Lhd-β RCs. For both mutants, the estimates are consistent with those obtained from D bleaching in the 850-nm region.

We turn now to identify the states that give rise to the spectra observed in Mhd-β and Lhd-β RCs following D* decay. The clear candidate choices are $D^+\beta^-$ or $D^+H_M^-$ or a mixture of these L- and M-side states, which, in fact, appears to be the case. We consider first the data for Lhd-β RCs, where the evidence for electron transfer to H_M is more clear (Figure 7B) and then turn to the Mhd-β data in Figure 7A, which is the more difficult case to evaluate because of spectral overlap of the H_M and D bleachings and a lower overall yield of charge separation from D*.

Three spectra are compared in Figure 7B: the D* spectrum (green, which is identical for the Lhd and Lhd-β RCs), the 100-ps Lhd spectrum (blue), and the 135-ps Lhd-β spectrum (red). Considerable signal averaging went into the spectra for this comparison, and the amplitudes of the features in the Lhd-β spectrum served as (an arbitrary) a reference for normalization of the other two spectra. The signal-to-noise of the D* spectrum is far superior to the other two simply because it is so much larger in original amplitude (i.e., most of D* decays to the ground state and not to charge-separated products). First, we consider the D* (0.5 ps) and 100-ps spectrum of Lhd RCs, which was assigned above to $D^+H_L^-$ with little evidence for reduction of H_M. These data argue the reason for this assignment. As described above, the 100-ps Lhd spectrum reveals a Q_X bleaching that is slightly blue-shifted compared to that of D*, in keeping with reduction of H_L (and co-bleaching of D). Continuing the comparison further to the blue, the shapes of the two spectra are very similar. There is no evidence of H_M bleaching at 528 nm in the 0.5-ps D* spectrum, and none is expected. Using this as a reference, it is seen that the 100-ps spectrum for Lhd RCs is nearly identical to the D* spectrum in the vicinity of 528 nm. In contrast, the 135-ps for the Lhd-β mutant (red) shows clear evidence of bleaching at 528 nm, which we take as evidence for electron transfer from D* to H_M to form $D^+H_M^-$. Additionally, there is a distinct increased absorption in the 640−650 nm region in the Lhd-β versus Lhd spectra, again consistent with formation of the H_M anion in the former RC.

Estimating the yield of $D^+H_M^-$ in the Lhd-β RC is difficult because of the small H_M bleaching at 528 nm, overlap with bleaching of the BPh component of D at 552 nm, and the lack of a "standard" known bleaching amplitude as a reference. However, we do have known difference spectra of the H_M Q_X bleaching at 528 nm for state $P^+H_M^-$ in 30% yield in the YFH mutant.[8] Using that known spectrum and the D* spectrum of Lhd acquired here, and assuming that the 552-nm extinction coefficient of D is the same as that of a monomer BPh, we have simulated the *shape* of the 135-ps spectrum of Lhd-β RCs in Figure 7B between 520 and 560 nm. Independently, we fit the bleaching profile with a sum of two Gaussians. On the basis of these analyses, we estimate that of the ∼15% total charge-

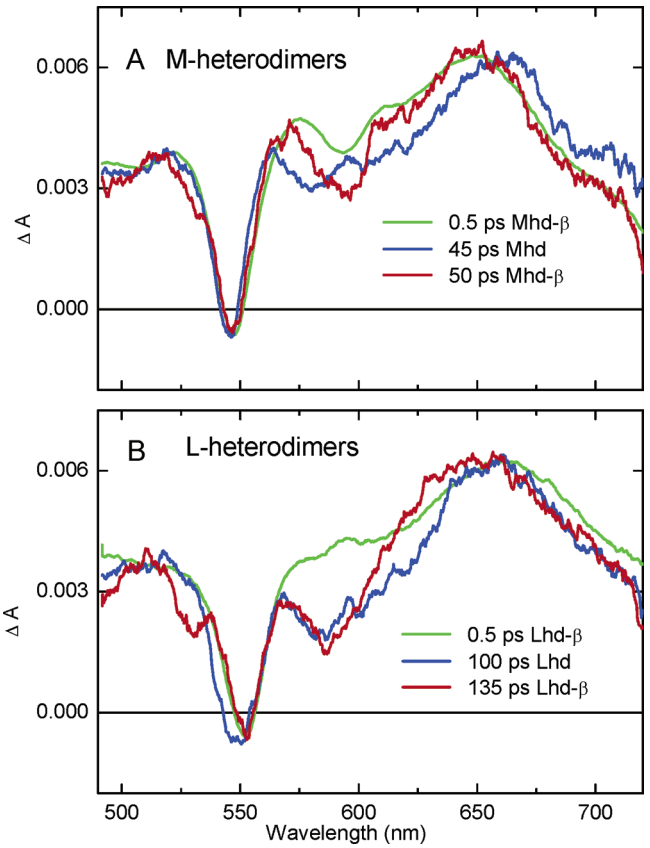

Figure 7. Comparison of the visible-region transient absorption spectra for (A) the Mhd and Mhd-β mutants and (B) the Lhd and Lhd-β mutants. The spectra were acquired at the times indicated following excitation with a 130-fs 850-nm excitation flash and have been normalized for comparison purposes. See the text for further details.

separated products of D* decay in the Lhd-β mutant, ~40% is due to $D^+H_M^-$. We presume that the remaining 60% forms $D^+\beta^-$ on the L side. Thus, we estimate the absolute yields of the products of D* decay in Lhd-β RCs are 85% ground-state recovery, 9% $D^+\beta^-$ and 6% $D^+H_M^-$. A branching ratio of 3/2 is thus obtained for D* electron transfer to the L/M sides of the RC in the Lhd-β mutant. To the extent to which the assumption about extinction coefficients does not hold, the relative yields of $D^+H_M^-$ and $D^+\beta^-$ would have to be adjusted, but their combined yield is limited to 15%.

The Lhd and Lhd-β RCs are the most amenable to discerning spectral evidence for formation of $D^+H_M^-$ because the position of the Q_X bleaching of D* is at 552 nm and the D* anion peak is near 660 nm. In contrast, for the Mhd and Mhd-β RCs the Q_X bleaching of D* is at 547 nm and its anion-region feature is at 650 nm, making spectral changes associated with formation of H_M^- more challenging to resolve. The spectral comparison in Figure 7A for the Mhd RCs parallels that described above for the Lhd RCs. The D* spectrum (again identical for the Mhd and Mhd-β RCs) at 0.5 ps is shown in green. The 50-ps spectrum for the Mdh RC (blue) is again essentially identical to that for D* in the vicinity of 528 nm. The 50-ps spectrum for the Mhd-β RC (red) shows a very slight shoulder on the blue side of the 547-nm bleaching. Because this shoulder is not seen in either the D* spectrum or in the 45-ps spectrum of Mhd RCs, we take this as indicating some electron transfer from D* to H_M to form $D^+H_M^-$ in the Mhd-β RC. Using the procedures described above for analysis of the spectra for Lhd-β RCs, we estimate that of the ~7% (total) yield of charge-separated products from D*, ~20% is $D^+H_M^-$ and ~80% is $D^+\beta^-$. Thus, the absolute yields of the products of D* decay in Mhd-β RCs are 93% ground-state recovery, 5.5% $D^+\beta^-$, and 1.5% $D^+H_M^-$. Thus, a branching ratio of 4/1 is obtained for D* electron transfer to the L/M sides of the Mhd-β RC.

Because the data were analyzed in exactly the same manner, we believe that the 4/1 branching ratio for L/M electron transfer in the Mhd-β RC is significantly different than the 3/2 ratio for the Lhd-β RC. Thus, despite the difficulties associated with accurately determining the small absolute yields of electron transfer from D* to the M side in both mutants, it is clear that there is a higher yield of $D^+H_M^-$ in the Lhd-β mutant than in the Mhd-β mutant. In the next section, these yields are coupled with the D* lifetimes to obtain estimates for the rate constants for electron transfer from D* to the L and M sides of the RC. Comparison of the rate constants with each other and with those from other RCs affords further insight into the origin of the directionality of charge separation.

Discussion

Ground-State Absorption Properties of D. The near-infrared absorption characteristics of D have been discussed previously by a number of workers.[51,60,63,71,85,86] As has been noted for the *R. sphaeroides* heterodimer mutants, the *R. capsulatus* Lhd RC has a somewhat narrower and more resolved absorption feature near 850 nm, compared to the broader and more featureless absorption of D in the Mhd mutant. This difference ultimately derives from contributions of two underlying heterodimer excited states to the near-infrared absorption of D, the lower-energy one with more CT character and the higher-energy one with more exciton character.

For technical reasons, previous picosecond transient absorption studies on the heterodimer mutants did not probe the region between ~580 and ~620 nm. Thus, the bleaching features for state D* in the transient difference spectra in Figures 4 and 6 provide new insight into the ground-state absorption properties of the heterodimers in this region of the spectrum. From the D* difference spectra, it is seen that the Mhd possesses only a little BChl-like oscillator strength near 600 nm and the Lhd has essentially none. For both heterodimers, the major Q_X oscillator strength of D is more BPh-like, occurring at 547 nm for the Mhd and at 552 nm for the Lhd. This conclusion comes from the observed positions and amplitudes of D bleaching at 0.5 ps, and provides information on absorption properties of D not obtained readily from the ground-state spectra. This analysis assumes that effects such as the CT nature of D* do not cause (inordinately large) electrochromic shifts of the B_L and B_M bands in the difference spectra that fortuitously cancel the true bleaching of D in the 580−620 nm window. Absent such effects, the general finding is that the Lhd largely possesses a single BPh Q_X-like band at 552 nm with an ~22 nm fwhm. This feature is red-shifted and broader than the Q_X absorption bands of H_M (528 nm, 17 nm fwhm) and H_L (542 nm, 16 nm fwhm). The Mhd differs further, with a main band at 547 nm (~19 nm fwhm) and a second much weaker band at ~592 nm. These features would be interesting to reproduce in simulations of the full ground state spectra of heterodimer RCs, which thus far have concentrated on the near-infrared region. Such simulations would potentially provide additional information on the electronic structure of the heterodimer.

Primary Charge Separation in Heterodimer and Heterodimer-β RCs. The new heterodimer-β mutants reported here possess a number of characteristics discussed in the Introduction that make them well suited to obtain further insight into the relative contributions of the Franck−Condon (energetic) factor and electronic matrix elements to the rates of electron transfer

TABLE 1: P* or D* Lifetimes, Yields of Decay Pathways, and Associated Rate Constants[a]

RC	P* or D* lifetime (ps)	% yield ground state	% yield L-side electron transfer	% yield M-side electron transfer	$(k_G)^{-1}$ (ps)	$(k_L)^{-1}$ (ps)	$(k_M)^{-1}$ (ps)
Lhd-β	40 ± 8	85	9	6	47	440	670
Mhd-β	15 ± 4	93	5.5	1.5	16	270	1000
Lhd	25 ± 5	70	30	n.d.	36	83	
Mhd	14 ± 4	75	25	n.d.	19	56	
YFH	11 ± 2	10	60	30	110	18	37
YF	8 ± 2	10	75	15	80	11	53
KDH	15 ± 2	15	62	23	100	24	65
DH	15 ± 2	15	70	15	100	21	100
H	8.5 ± 0.8	n.d.	93	7	$\sim$100[b]	8.6	114
wt	4.3 ± 0.3	n.d.	100	n.d.	$\sim$100[b]	4.2	$\sim$100[c]

[a] All data were recorded with *R. capsulatus* RCs at $\sim$285 K; n.d. = not detected. The results for wild-type (wt), H, DH, KDH, YFH, and YF RCS were taken from the literature.[5−8,10] The "H" in the H, DH, KDH, and YFH RCs indicates the substitution of His (H) for Leu(M212), placing a His over one face of the L-side BPh acceptor, H_L, and resulting in its replacement by a BChl (β). This is the same mutation present in the Mhd-β and Lhd-β RCs studied here. The "Y" in the YFH and YF RCs refers to the substitution of Tyr (Y) for Phe L181. This residue is situated near P and B_M, and a Tyr at L181 stabilizes $P^+B_M^-$. The "F" in the YFH and YF RCs refers to the substitution of Phe (F) for Tyr M208. This site is C_2 symmetry-related to L181, and a Phe at M208 destabilizes $P^+B_L^-$. The "K" in the KDH RC indicates the substitution of Lys (K) for Ser L178, placing a Lys near ring V of B_M and thus stabilizing $P^+B_M^-$. The "D" in the KDH and DH RCs is the substitution of Asp (D) for Gly M201 located near ring V of B_L and destabilizing $P^+B_L^-$. [b] The value has not been determined experimentally; however, to a first approximation, k_G for the H and wild-type RCs should be the same as that determined for DH, KDH, and YFH RCs because P should have the same electronic character. [c] The value has not been determined experimentally; however, to a first approximation, k_M for wild-type RC should be the same as that determined for DH and H RCs because the environments of P and the M-side cofactors are the same.

to the L and M sides of the RC. Table 1 summarizes the results on the Mhd-β and Lhd-β RCs and on the Lhd and Mhd single mutants. Results are also given for wild-type RCs and several other relevant mutants studied previously whose identities are defined in the footnotes to the table. The key experimental results in columns 2−5 of Table 1 are the lifetime (τ) of the excited primary electron donor (P* for the wild-type BChl-BChl dimer or D* for the BChl-BPh heterodimers) and the yields (ϕ_i) of the three observed products of P*(D*) decay. Using these data and a simple branching model, the rate constants (k_i) for P*(D*) internal conversion to the ground state (k_G), electron transfer to the L side (k_L), and electron transfer to the M side (k_M) were calculated from the formula $k_i = \phi_i/\tau$. These rate constants are given in columns 6−8 of the Table. In the following, we first discuss D* internal conversion to the ground state, then electron transfer to the L side, and electron transfer to the M side as framework for comparing the rates of electron transfer to the two branches in the heterodimer RC with wild-type and other mutant RCs.

Internal Conversion of D* to the Ground State. The rate of internal conversion to the ground state gives a measure of the contribution of the $D_L^+D_M^-$ and $D_L^-D_M^+$ CT configurations (along with the $D_L^*D_M$ and $D_LD_M^*$ locally excited configurations) to D*, and similarly for P*. As has been discussed previously for the heterodimers, this arises because nonradiative deactivation of an excited strongly coupled dimer can be enhanced by Born−Oppenheimer breakdown. This coupling of nuclear and electronic degrees of freedom is associated with motions that modulate the distance between the two macrocycles and their Coulombic interactions, which in turn affect the energies of the CT configurations (more so than the locally excited configurations) that comprise the wave function of the lowest excited state.[56,58,59,63] For example, the $D(BChl)_L^+D(BPh)_M^-$ CT configuration is greatly stabilized in the M heterodimer compared to $P(BChl)_L^+P(BChl)_M^-$ in the native dimer and is thought to make the dominant contribution to D* in the Mhd and Mhd-β mutants. No doubt, this increased CT character underlies the much larger rate constant of $\sim(15-20\ \text{ps})^{-1}$ for D* internal conversion compared to $\sim(100-200\ \text{ps})^{-1}$ for the wild-type BChl-BChl dimer, in which P* has predominantly exciton character. This assessment of the substantial (predominant) CT character of D* in the Mhd and Mhd−β mutants is consistent with the broad weak tail of the absorption extending past 900 nm in the ground-state spectrum (Figure 3A) and the stronger main portion of the near-infrared absorption at higher energy being due to the next highest excited state, which contains a greater admixture of the two locally excited configurations (i.e., more exciton character).

A similar correlation between D* CT character, ground-state absorption, and internal conversion rate constant applies to the L heterodimer. In both the Lhd and Lhd-β mutants, the D* internal conversion rate is $\sim(35-45\ \text{ps})^{-1}$, somewhat smaller than for the Mhd but still larger than for the wild-type dimer, P. This finding implies that there is less CT character of D* in the L heterodimer compared to the M−heterodimer. This view is consistent with the lowest charge-transfer configuration of D* being $D(BPh)_L^-D(BChl)_M^+$, which may not be stabilized as much as $D(BChl)_L^+ D(BPh)_M^-$ in the M heterodimer, thus giving a smaller net CT contribution to the wave function for D* in the L heterodimer. This reduced stabilization is anticipated because the nascent CT character provided by the environment (as in wild-type) is thought to be in the direction favoring $D_L^+D_M^-$.[24,25,27,28,39,53,54] A reduced CT character and slower D* internal conversion rate in the L versus M heterodimer RCs is consistent with the ground-state spectra of the L heterodimer being slightly more wild-type-like in displaying a somewhat more pronounced near-infrared absorption feature, indicating more exciton character to D* (see Figure 3 and also spectra in refs 53 and 60).

L-Side Electron Transfer from D*. In wild-type RCs, state $P^+B_L^-$ appears to be 50−100 meV below P*, facilitating a two-step electron-transfer process between P* and $P^+H_L^-$, possibly in parallel with a less pronounced role as a virtual intermediate in a superexchange mechanism. A number of mutations have been made that affect the environment of B_L and apparently raise the free energy of $P^+B_L^-$. Examples include the DH, KDH, YF, and YFH mutants, all of which have rate constants for electron transfer from P* to the L side that are reduced compared to wild-type (Table 1). We expect that in the heterodimer RCs, the fact that D is more difficult to oxidize by 140−180 meV than the wild-type P results in $D^+B_L^-$ being sufficiently far above D* in free energy so as to preclude the two-step mechanism (Figure 2C and D). Qualitatively, this model is confirmed by the much smaller rate constants for electron transfer to the L side by a superexchange mechanism in the heterodimer mutants. For the Lhd and Mhd mutants where the L-side acceptor is H_L, the values for k_L are $\sim(56-83\ \text{ps})^{-1}$ compared to $\sim(4\ \text{ps})^{-1}$ wild-type. For the Lhd-β and Mhd-β mutants where the L-side acceptor is β, the values for k_L are $\sim(270-440\ \text{ps})^{-1}$ compared to $\sim(9\ \text{ps})^{-1}$ the single H mutant.

The superexchange mechanism for electron transfer to the L side (and analogously to the M side discussed below) in the heterodimer-containing RCs depends on electronic mixing of the initial state (D*) and the final state ($D^+H_L^-$ in Mhd and Lhd RCs, and $D^+\beta^-$ in Mhd-β and Lhd-β RCs) with the virtual

intermediate $D^+B_L^-$. This mixing is commonly described in terms of first-order perturbation theory. Within this framework, the effective electronic mixing (coupling) for the overall L-side process in Mhd-β and Lhd-β RCs can be written

$$V_{D\beta} = [V_{DB}V_{B\beta}]/\Delta E_{D\beta} \quad (1a)$$

Here V_{DB} and $V_{B\beta}$ are the electronic matrix elements (that depend on spatial orbital overlaps and electron density distributions) between D* and $D^+B_L^-$ and between $D^+B_L^-$ and $D^+\beta^-$, respectively. The energy denominator, $\Delta E_{D\beta}$, is the energy (not free energy) gap between the potential energy surfaces for D* and $D^+\beta^-$ at the nuclear coordinate where the D* and $D^+B_L^-$ surfaces cross. The analogous effective electronic mixing for L-side electron transfer in Mhd and Lhd RCs also involve D* and $D^+B_L^-$ but with $D^+H_L^-$ as the final state and can be written

$$V_{DH} = [V_{DB}V_{BH}]/\Delta E_{DH} \quad (1b)$$

The superexchange rate constant ($k \propto V^2 \cdot FC$) will depend on the square of the effective electronic mixing (coupling) term, either $V_{D\beta}^2$ or V_{DH}^2, multiplied by the appropriate Franck−Condon factor (FC), which depends on the free energy gap between D* and $D^+\beta^-$ or $D^+H_L^-$ and the reorganization energy.

In comparing Mhd with Mhd-β RCs, the electronic matrix element, V_{DB}, is the same, and to a first approximation $V_{B\beta}$ in eq 1a should be the same as V_{BH} in eq 1b because the RC architecture (orientations and distances between the pigments) is essentially unperturbed by the substitution of β for H_L[80] and the electron density distribution in β and H_L should not differ significantly. The same observations hold true for the comparison between Lhd and Lhd-β RCs. Thus, the primary difference in the effective electronic mixing for these pairwise comparisons should derive from the energy denominator, with $D^+H_L^-$ in Mhd (or Lhd) RCs anticipated to be 100−200 meV lower in energy than $D^+\beta^-$ in Mhd-β (or Lhd-β) RCs. The free energy gap between D* and $D^+H_L^-$ versus $D^+\beta^-$ will also contribute to differences in Franck−Condon factors. The rate constants we determine in Table 1 for electron transfer from D* to the L side are $k_L = (56\ ps)^{-1}$ versus $(270\ ps)^{-1}$ for the Mhd and Mhd-β comparison and $(83\ ps)^{-1}$ versus $(440\ ps)^{-1}$ for Lhd and Lhd-β RCs. These results suggest that the energy denominator contributes a factor of ∼5 in modulating the superexchange rate constant for L-side electron transfer in heterodimer RCs with H_L versus β as the primary acceptor.

In making the other pairwise comparisons of interest, Mhd with Lhd RCs (both having H_L) and Mhd-β with Lhd-β RCs (both having β), the effective electronic couplings given by eqs 1a and b will differ primarily because of differences in the electronic matrix element, V_{DB}. This follows because the electron density distribution in D* is clearly different for the two heterodimers, weighted primarily to $D(BChl)_L^+D(BPh)_M^-$ for the M heterodimer and to $D(BPh)_L^-D(BChl)_M^+$ for the L heterodimer. There may also be small differences in the energy denominators derived from (small) differences in the energies of D*, $D^+B_L^-$, and $D^+\beta^-$ (or $D^+H_L^-$), the latter due to possible differences in the oxidation potential of D (∼20 mV difference based on the *R. sphaeroides* mutants[63,73]). However, we expect that these variations in energy denominators will be much less than those discussed above for replacing H_L with β. Our experimental results yield the comparisons of $k_L = (56\ ps)^{-1}$ with $(83\ ps)^{-1}$ for the Mhd and Lhd RCs, respectively, and $(270\ ps)^{-1}$ with $(440\ ps)^{-1}$ for Mhd-β and Lhd-β RCs, respectively. These comparisons indicate that differences between the electronic matrix elements (principally V_{DB}^2) of the two heterodimers result in at most a factor of 2 difference between the rate of electron transfer from D* to the L side of the RC. Our analysis also shows that the electron density distribution inherent in the M heterodimer is superior to that of the L heterodimer in supporting electron transfer to the L side, as determined from the comparisons of the value of k_L for Mhd with Lhd RCs and of Mhd-β with Lhd-β RCs. This point is discussed further below in the section comparing L- and M-side electron transfer in the heterodimer mutants.

M-Side Electron Transfer from D*. The working model of the wild-type RC places state $P^+B_M^-$ sufficiently above P* in free energy that electron transfer to the M side to form $P^+H_M^-$ is limited to the superexchange mechanism, with little or no possibility for a two-step process. The ∼100−150 meV increased oxidation potential of D in the heterodimer-containing RCs will raise $D^+B_M^-$ this much further above D* (Figure 2D). This will alter the superexchange rate from that in wild-type RCs via the energy denominator in the expressions analogous to eqs 1a and b for M-side electron transfer. Additionally, the different electron-density distributions in D* versus P* will modulate the rate via the electronic matrix element, V_{DB}, in the mutants versus the analogous element, V_{PB}, in wild-type RCs. These combined effects reduce the observed rate constants for electron transfer from D* to the M side by a factor of roughly 7−10 compared to the rate in the wild type, namely, $k_M = (670\ ps)^{-1}$ and $(1000\ ps)^{-1}$ for Lhd-β and Mhd-β RCs, respectively, compared to the value of $\sim(100\ ps)^{-1}$ estimated for wild-type RCs (Table 1).[87]

We can also compare the k_M values for the Mhd-β and Lhd-β RCs to gain insight into the differential relative electronic couplings of the two macrocycles of D* and $D^+H_M^-$, as mediated by $D^+B_M^-$. As before, any difference would derive from the opposite electron density distributions on the two macrocycles of D* in the L versus M heterodimers. Similar to the situation found above for the values of k_L, the values of k_M for Mhd-β and Lhd-β RCs differ from each other by only ∼50%. And again, this gives an upper limit on the differences in the effective superexchange mixing (coupling) elements because possible small differences in superexchange energy denominators and Franck−Condon factors may also come into play. Using the same logic as described above for D* electron transfer to the L side, we expect that the principal difference in electronic mixing will depend on the square of the electronic matrix element, V_{DB} (involving D* and $D^+B_M^-$). Again, this result is similar to that described for L-side electron transfer in suggesting only a relatively small difference between the electronic matrix elements of the two macrocycles of D and the M-side cofactors. However, opposite to the situation found for electron transfer to the L side, M-side electron transfer appears to be facilitated by having electron density on the L macrocycle of the primary donor. Again, this point will be elaborated further below.

Comparison of Electron Transfer from D* to the L versus M Sides. As described in the Introduction, a central question underlying the present study is the extent to which differences in the L- versus M-side electronic factors (derived from the wave functions, orbital overlaps, electron density distributions) supplement energetic factors (free energy differences, reorganization energies, one- versus two-step mechanisms) in dictating the relative rates of electron transfer to the L and M branches in the native RC. Our results on the L and M heterodimer-β RCs yield fundamental information on this issue by providing a comparison of rate constants for electron transfer to the L versus M sides in mutants in which (1) the mechanism is the same and no doubt is solely superexchange on both branches, (2) the

ultimate acceptor states on the two branches have much more comparable free energies than in wild-type RCs, and (3) the electron density is preferentially weighted to one macrocycle or the other in the excited primary electron donor (D*). The latter gross differential CT weighting means that electron-density contributions (along with orbital overlaps) to the electronic couplings between D* and the charge-separated states on the two branches will be magnified in the mutants compared to wild-type RCs, where charge is distributed more (but not exactly) equally between the two macrocycles of P*. Thus, comparisons of L- versus M-side electronic contributions in the opposite heterodimer mutants should provide an upper limit to the corresponding differences that may be present in the wild-type RC.

The direct comparisons that can be made relevant to these issues are for the two heterodimer-β RCs where electron transfer to the M side is observed, albeit in very low yield. The rate constants we determine are $k_L = (270\ \text{ps})^{-1}$ versus $k_M = (1000\ \text{ps})^{-1}$ for Mdh-β RCs and $k_L = (440\ \text{ps})^{-1}$ versus $k_M = (670\ \text{ps})^{-1}$ for Ldh-β RCs. The fact that these rates are minimally 60-fold smaller than $k_L \approx (4\ \text{ps})^{-1}$ for wild-type RCs is consistent with the superexchange mechanism operating exclusively on both sides in these RCs. The $k_L/k_M \approx 4$ rate ratio for Mhd-β and $k_L/k_M \approx 1.5$ for Lhd-β show that the L side is favored in both mutants, but again, more so in the Mhd-β mutant. This ratio can be recast in terms of effective electronic mixing (V^2) and Franck−Condon (FC) factors for the two sides and generally written $k_L/k_M = [V_L^2 FC_L]/[V_M^2 FC_M]$, where the V elements are given by the appropriate versions of eq 1a for the two branches. Because the free energy gaps between D* and the acceptor states on the two sides ($D^+\beta^-$ versus $D^+H_M^-$) are expected to be comparable, and assuming comparable reorganization energies, the FC_L/FC_M ratio is probably close to unity. This is entirely plausible because of the fact that FC_L/FC_M has been calculated to be only ~1.5 for wild-type RCs under models of a superexchange mechanism for electron transfer to both sides of the RC.[27,28] This analysis indicates that a factor of 4 can be taken as an upper limit on the ratio of the effective superexchange electronic mixings V_L^2/V_M^2 in heterodimer-containing RCs.

The general conclusion that $V_L^2 > V_M^2$ is consistent with electronic structure calculations carried out by Zhang and Friesner on heterodimer RCs.[26] Their calculations, which included the CT configurations that are key to defining the character of D*, showed a larger electronic coupling between D* and B_L than between D* and B_M for *both* heterodimers. These authors also found for both heterodimer and wild-type RCs, as discussed previously for wild-type,[25,28,30] that the M macrocycle of the primary electron donor has a stronger electronic interaction with B_L than B_M, and vice versa for the L macrocycle of the dimer; a significant contribution to these differences arises from the distances involved.

Our findings for the heterodimer RCs agree fully with these previous conclusions, underscoring the methods we used to analyze the data and the general relationships found between rate constants for electron transfer from D* to the L and M sides in these mutants reported in Table 1. As mentioned above, the comparison of rate constants k_L and k_M for the Mhd-β and Lhd-β RCs clearly suggests that a design criterion to bias electron transfer to the L side in the native RC would be to have the electrostatics of the protein endow P* with some net $P_L^+P_M^-$ CT character in order to weight electron density away from the L macrocycle and toward the M macrocycle, which has the better coupling to the L branch. This is, in fact, the direction of net CT character of P* that has been indicated from a number of studies.

Extrapolations to the Origins of Directionality in the Wild-Type RC. In assuming for this discussion that our findings of $k_L/k_M \approx 4$ for Mhd-β RCs and ≈1.5 for Lhd-β RCs provide a reasonable general upper limit of $V_L^2/V_M^2 \approx 4$ for the ratio of effective L- versus M-side electronic couplings in heterodimer-containing RCs, we consider now how this result can be extrapolated to assess how much difference there is between V_L^2 and V_M^2 in wild-type RCs. At the core, the question is how much does V_L^2/V_M^2 contribute to the ratio of rates $k_L/k_M \approx 30$ for the wild-type RC, and how much of this factor of 30 bias is contributed by FC_L/FC_M. Before we can make this extrapolation, we first discuss the findings of some previous calculations on wild-type RCs that include the possibility of interference effects, which would be much different for wild-type and heterodimer RCs.

A number of theoretical studies have calculated large asymmetries in the electronic-coupling contributions to the L versus M sides that, at face value, could account largely, if not entirely, for the unidirectionality of electron transfer in the wild-type RC.[28,30] For example, in one study of superexchange mechanisms on the two branches in wild-type RCs, it was found that the ratio of electronic matrix elements $V^2_{P^*\rightarrow P+B_L^-}/V^2_{P^*\rightarrow P+B_M^-} = 7.7$, and the ratio between $V^2_{P+B_L^-\rightarrow P+H_L^-}/V^2_{P+B_L^-\rightarrow P+H_M^-} = 4.3$. The product gives an overall electronic contribution $V_L^2/V_M^2 = 33$, thus fully accounting for the ratio of 30 for k_L/k_M (assuming equal energy denominators in the superexchange formulas analogous to eq 1b).[28] However, it has been noted that prescriptions for the effective electronic couplings may be more complex because of possible destructive interference effects.[26,30] In particular, because P* is dominated by the asymmetric exciton configuration ($P_L^*P_M - P_LP_M^*$), the net electronic coupling to $P^+B_L^-$ on the L side should involve *subtraction* of the respective electronic matrix elements, namely, $V^2_{P_L^*P_M\rightarrow P+B_L^-} - V^2_{P_LP_M^*\rightarrow P+B_L^-}$. According to the calculations,[26,30] this difference is large, leaving a significant net electronic coupling between P* and $P^+B_L^-$. In other words, there is little destructive interference effect on the L side. However, subtraction of the M-side electronic matrix elements, namely, $V^2_{P_L^*P_M\rightarrow P+B_M^-} - V^2_{P_LP_M^*\rightarrow P+B_M^-}$, gives a value near zero, leading to a much smaller net electronic coupling between P* and $P^+B_M^-$. In other words, there is substantial destructive interference effect on the M side. It is suggested that such a difference in destructive interference effects on the two sides may be a substantial source of unidirectionality in the native RC favoring the L side.

In principle, such interference effects should be less significant for the heterodimer-containing RCs than for the wild-type. This owes to the wave function for D* being weighted much more heavily by a single CT configuration, namely, $D(BChl)_L^+D(BPh)_M^-$ for the M heterodimer and $D(BPh)_L^-D(BChl)_M^+$ for the L heterodimer, and having much less of the $P_L^*P_M - P_LP_M^*$ exciton character. We can obtain insight into the possible magnitudes of the interference effects for the heterodimer RCs from the data in Table 1. The rate constants for electron transfer from $D^* \rightarrow D^+H_M^-$ $(670-1000\ \text{ps})^{-1}$ for Ldh-β and Mdh-β RCs are roughly 7−10 times smaller than $k_M \approx (100\ \text{ps})^{-1}$ estimated for wild-type RCs. This 7- to 10-fold difference could reflect the elimination of the interference effect on the M-side electronic coupling in the mutants, providing an upper limit to the effect. Alternatively, the difference could reflect differences in the superexchange energy denominator, deriving from the shifting of the free energy levels of the charge-separated states because of the greater oxidation

potential of D versus P. The L-side rate constants in Table 1 help discern the magnitude of an energy-denominator effect. The appropriate reference point here is RCs containing a wild-type dimer, containing β in place of H_L, and in which the two-step mechanism is greatly reduced or (best) eliminated. The DH, KDH, and YFH mutants best fulfill these criteria. Here, the $\sim$10−20-fold reduction of k_L from $\sim(20\ \text{ps})^{-1}$ in these RCs to $(270-440\ \text{ps})^{-1}$ for the Mhd-β and Lhd-β RCs must be due substantially or completely to a reduction in the superexchange energy denominator, because for the L side (according to the calculations discussed above) there is little destructive interference effect in the first place for P*. Because the $\sim$10−20-fold change in k_L for the DH, KDH, and YHF mutants compared to the Mhd-β and Lhd-β mutants is the same as we find for in the change in k_M for the same RCs ($\sim(37-100\ \text{ps})^{-1}$ compared to $(670-1000\ \text{ps})^{-1}$), one could argue that there is *not* much of a contribution from the *loss* of an interference effect on k_L/k_M in going from the wild-type dimer P to the heterodimer D as the primary electron donor. Collectively, these considerations would imply in turn that destructive interference effects on electronic coupling do not make a substantial contribution to directionality in the wild-type RC. However, more theoretical and experimental work needs to be done before a firm conclusion on this point can be reached.

We conclude with some general remarks regarding the upper limit $V_L^2/V_M^2 \approx 4$ that we have obtained for the ratio of effective L- versus M-side superexchange electronic mixing (coupling) terms for heterodimer-containing RCs. The key conclusions based on this ratio and the collective considerations given above are as follows: (1) The L- versus M-side electronic mixings in the heterodimer mutants should represent an upper limit on the differences in wild-type RCs, where the electron density distribution in the excited primary electron donor is more balanced. (2) The contribution of V_L^2/V_M^2 to k_L/k_M in wild-type RCs would not be expected to be more than a factor of $\sim$4 (assuming little contribution of potential interference effects). (3) In comparison to the $k_L/k_M \approx 30$ for wild-type RCs obtained from early work[18,19] and rate constants derived from mutants (Table 1),[5,6,8,9] this leaves a factor of $\sim$7 for the minimum contribution of the relative free energies (and reorganization energies) of the L- versus M-side states such as $P^+B_L^-$ versus $P^+B_M^-$ (and $D^+H_L^-$ versus $D^+H_M^-$), including the relative contributions of one- and two-step mechanisms on the two branches. These results suggest that the electronic factors contribute $\sim$35% at most to directionality with the other 65% deriving from energetic considerations. A similar conclusion was reached from work on the YFH mutant, where it was suggested that electronic interactions contribute a factor of 2−7 out of the overall factor of 30 for directionality in the wild-type RC.[8] Taken together, these results suggest that the electronic contribution to directionality is most comparable to that of energetic factors. In other words, the electronic couplings are not overwhelmingly dominant and supplement the contribution of energetic factors demonstrated from studies on a number of mutant RCs. In addition to these general conclusions, the results presented here should be valuable in the design of additional mutants and in further theoretical treatments to help elucidate even more precisely the contributions to the directionality of electron transfer in photosynthetic proteins.

Acknowledgment. This work was supported by Grant MCB-0314588 from the National Science Foundation (C.K. and D.H.) and the U.S. Department of Energy, Office of Biological and Environmental Research, under contract no. W-31-109-ENG-38 (P.D.L. and D.K.H).

References and Notes

(1) Deisenhofer, J.; Epp, O.; Miki, K.; Huber, R.; Michel, H. *Nature* **1985**, *318*, 618−624.
(2) Allen, J. P.; Feher, G.; Yeates, T. O.; Komiya, H.; Rees, D. C. *Proc. Natl. Acad. Sci. U.S.A.* **1987**, *84*, 5730−5734.
(3) Chang, C.-H.; El-Kabbani, O.; Tiede, D. M.; Norris, J. R.; Schiffer, M. *Proc. Natl. Acad. Sci. U.S.A.* **1991**, *30*, 5352−5360.
(4) Ermler, U.; Fritsch, G.; Buchanan, S. K.; Michel, H. *Structure* **1994**, *2*, 925−936.
(5) Heller, B. A.; Holten, D.; Kirmaier, C. *Science* **1995**, *269*, 940−945.
(6) Kirmaier, C.; Weems, D.; Holten, D. *Biochemistry* **1999**, *38*, 11516−11530.
(7) Roberts, J. A.; Holten, D.; Kirmaier, C. *J. Phys. Chem. B* **2001**, *105*, 5575−5584.
(8) Kirmaier, C.; He, C.; Holten, D. *Biochemistry* **2001**, *40*, 12132−12139.
(9) Kirmaier, C.; Laible, P. D.; Hanson, D. K.; Holten, D. *Biochemistry* **2003**, *42*, 2016−2024.
(10) Kirmaier, C.; Laible, P. D.; Hanson, D. K.; Holten, D. *J. Phys. Chem. B* **2004**, *108*, 11827−11832.
(11) Katilius, E.; Turanchik, T.; Lin, S.; Taguchi, A. K. W.; Woodbury, N. W. *J. Phys. Chem. B* **1999**, *103*, 7386-7389.
(12) Katilius, E.; Babendure, J. L.; Katiliene, Z.; Lin, S.; Taguchi, A. K.; Woodbury, N. W. *J. Phys. Chem. B* **2003**, *107*, 12029−12034.
(13) Haffa, A. L. M.; Lin, S.; Williams, J. C.; Bowen, B. P.; Taguchi, A. K. W.; Allen, J. P.; Woodbury, N. W. *J. Phys. Chem. B* **2004**, *108*, 4−7.
(14) de Boer, A. L.; Neerken, S.; de Wijn, R.; Permentier, H. P.; Gast, P.; Vijgenboom, E.; Hoff, A. J. *Biochemistry* **2002**, *41*, 3081−3088.
(15) de Boer, A. L.; Neerken, S.; de Wijn, R.; Permentier, H. P.; Gast, P.; Vijgenboom, E.; Hoff, A. J. *Photosynth. Res.* **2002**, *71*, 221−239.
(16) Lin, S.; Jackson, J. A.; Taguchi, A. K. W.; Woodbury, N. W. *J. Phys. Chem. B* **1999**, *103*, 4757−4763.
(17) Haffa, A. L. M.; Lin, S.; Williams, J. C.; Taguchi, A. K. W.; Allen, J. P.; Woodbury, N. W. *J. Phys. Chem. B* **2003**, *107*, 12503−12510.
(18) Bixon, M.; Jortner, J.; Michel-Beyerle, M. E.; Ogrodnik, A. *Biochim. Biophys. Acta* **1989**, *977*, 273−286.
(19) Kellogg, E. C.; Kolaczkowski, S.; Wasielewski, M. R.; Tiede, D. M. *Photosynth. Res.* **1989**, *22*, 47−59.
(20) Laible, P. D.; Kirmaier, C.; Holten, D.; Tiede, D. M.; Schiffer, M.; Hanson, D. K. Formation of $P^+Q_B^-$ via B−Branch Electron Transfer in Mutant Reaction Centers. In *Photosynthesis: Mechanisms and Effects*; Garab, G., Ed.; Kluwer Academic Publishers: Dordrecht, The Netherlands, 1998; pp 849−852.
(21) Breton, J.; Wakeham, M. C.; Fyfe, P. K.; Jones, M. R.; Nabedryk, E. *Biochim. Biophys. Acta* **2004**, *1656*, 127−138.
(22) Wakeham, M. C.; Jones, M. R. *Mechanisms of Bioenergetic Membrane Proteins* **2005**, *133*, 851−857.
(23) King, B. A.; deWinter, A.; McAnaney, T. B.; Boxer, S. G. *J. Phys. Chem. B* **2001**, *105*, 1856−1862.
(24) Parson, W. W.; Chu, Z. T.; Warshel, A. *Biochim. Biophys. Acta* **1990**, *1017*, 251−272.
(25) Scherer, P. O. J.; Fischer, S. F. *Chem. Phys.* **1989**, *131*, 115−127.
(26) Zhang, L. Y.; Friesner, R. A. *Proc. Natl. Acad. Sci. U.S.A.* **1998**, *95*, 13603−13605.
(27) Michel-Beyerle, M. E.; Plato, M.; Deisenhofer, J.; Michel, H.; Bixon, M.; Jortner, J. *Biochim. Biophys. Acta* **1988**, *932*, 52−70.
(28) Plato, M.; Mobius, K.; Michel-Beyerle, M. E.; Bixon, M.; Jortner, J. *J. Am. Chem. Soc.* **1988**, *110*, 7279−7285.
(29) Hasegawa, J.; Nakatsuji, H. *J. Phys. Chem. B* **1998**, *102*, 10420−10430.
(30) Kolbasov, D.; Scherz, A. *J. Phys. Chem. B* **2000**, *104*, 1802−1809.
(31) Rautter, J.; Lendzian, F.; Lubitz, W.; Wang, S.; Allen, J. P. *Biochemistry* **1994**, *33*, 12077−12084.
(32) Lendzian, F.; Huber, M.; Issacson, R. A.; Endeward, B.; Plato, M.; Bonigk, B.; Mobius, K.; Lubitz, W.; Feher, G. *Biochim. Biophys. Acta* **1993**, *1183*, 139−160.
(33) Parson, W. W.; Warshel, A. *J. Am. Chem. Soc.* **1987**, *109*, 6152−6163.
(34) Reimer, J. R.; Hush, N. S. *Chem. Phys.* **1995**, *197*, 323−334.
(35) Friesner, R.; Won, Y. *Biochim. Biophys. Acta* **1989**, *977*, 99−122.
(36) Thompson, M. A.; Zerner, M.; Fajer, J. *J. Phys. Chem.* **1991**, *95*, 5693−5700.
(37) Thompson, M. A.; Zerner, M. *J. Am. Chem. Soc.* **1991**, *113*, 8210−8215.
(38) Lockhart, D. J.; Boxer, S. G. *Proc. Natl. Acad. Sci. U.S.A.* **1988**, *85*, 107−111.
(39) Lathrop, E. J. P.; Friesner, R. A. *J. Phys. Chem.* **1994**, *98*, 6−3066.

(40) Meech, S. R.; Hoff, A. J.; Wiersma, D. A. *Proc. Natl. Acad. Sci. U.S.A.* **1986**, *83*, 9464−9468.
(41) Boxer, S. G.; Middendorf, T. R.; Lockhart, D. J. *FEBS Lett.* **1986**, *200*, 237−241.
(42) Tang, D.; Jankowiak, R.; Small, G. J.; Tiede, D. M. *Chem. Phys.* **1989**, *131*, 99−113.
(43) Won, Y.; Friesner, R. *J. Phys. Chem.* **1988**, *92*, 2214−2219.
(44) Losche, M.; Feher, G.; Okamura, M. Y. *Proc. Natl. Acad. Sci. U.S.A.* **1987**, *84*, 7537−7541.
(45) Scherer, P. O. J.; Fischer, S. F. *Chem. Phys. Lett.* **1986**, *131*, 153−159.
(46) Thurnauer, M.; Katz, J. J.; Norris, J. R. *Proc. Natl. Acad. Sci. U.S.A.* **1975**, *72*, 3270−3274.
(47) Takiff, L.; Boxer, S. G. *Biochim. Biophys. Acta* **1988**, *932*, 325−334.
(48) Dijkman, J. A.; den Blanken, H. J.; Hoff, A. J. *Isr. J. Chem.* **1989**, *28*, 141−148.
(49) Norris, J. R.; Budil, D. E.; Gast, P.; Chang, C.-H.; El-Kabbani, O.; Schiffer, M. *Proc. Natl. Acad. Sci. U. S. A.* **1989**, *86*, 4335−4339.
(50) Warshel, A.; Creighton, S.; Parson, W. W. *J. Phys. Chem.* **1988**, *92*, 2696−2701.
(51) Won, Y.; Friesner, R. *Biochim. Biophys. Acta* **1989**, *935*, 9−18.
(52) Boxer, S. G.; Goldstein, R. A.; Lockhart, D. J.; Middendorf, T. R.; Takiff, L. *J. Phys. Chem.* **1989**, *93*, 8280−8294.
(53) Moore, L. J.; Zhou, H.; Boxer, S. G. *Biochemistry* **1999**, *38*, 11949−11960.
(54) Gunner, M. R.; Nicholls, A.; Honig, B. *J. Phys. Chem.* **1996**, *100*, 4277−4291.
(55) Bylina, E. J.; Youvan, D. C. *Proc. Natl. Acad. Sci. U.S.A.* **1988**, *85*, 7226−7230.
(56) Kirmaier, C.; Holten, D.; Bylina, E. J.; Youvan, D. C. *Proc. Natl. Acad. Sci. U.S.A.* **1988**, *85*, 7562−7566.
(57) Fajer, J.; Borg, D. C.; Forman, A.; Dolphin, D.; Felton, R. H. *J. Am. Chem. Soc.* **1973**, *95*, 2739−2741.
(58) Kirmaier, C.; Bylina, E. J.; Youvan, D. C.; Holten, D. *Chem. Phys. Lett.* **1989**, *159*, 251−257.
(59) McDowell, L. M.; Kirmaier, C.; Holten, D. *Biochim. Biophys. Acta* **1990**, *1020*, 239−246.
(60) McDowell, L. M.; Gaul, D.; Kirmaier, C.; Holten, D.; Schenck, C. C. *Biochemistry* **1991**, *30*, 8315−8322.
(61) McDowell, L. M.; Kirmaier, C.; Holten, D. *J. Phys. Chem.* **1991**, *95*, 3379−3383.
(62) Laporte, L.; Mcdowell, L. M.; Kirmaier, C.; Schenck, C. C.; Holten, D. *Chem. Phys.* **1993**, *176*, 615−629.
(63) Laporte, L. L.; Palaniappan, V.; Davis, D. G.; Kirmaier, C.; Schenck, C. C.; Holten, D.; Bocian, D. F. *J. Phys. Chem.* **1996**, *100*, 17696−17707.
(64) Bylina, E. J.; Kolaczkowski, S. V.; Norris, J. R.; Youvan, D. C. *Biochemistry* **1990**, *29*, 6203−6210.
(65) Huber, M.; Lous, E. J.; Isaacson, R. A.; Feher, G.; Gaul, D.; Schenck, C. In *Reaction Centers of Photosynthetic Bacteria*; Michel-Beyerle, M.-E., Ed.; Springer: Berlin, 1990; pp 219−228.
(66) Huber, M.; Isaacson, R. A.; Abresch, E. C.; Gaul, D.; Schenck, C. C.; Feher, G. *Biochim. Biophys. Acta* **1996**, *1273*, 108−128.
(67) Hammes, S. L.; Mazzola, L.; Boxer, S. G.; Gaul, D. F.; Schenck, C. C. *Proc. Natl. Acad. Sci. U.S.A.* **1990**, *87*, 5682−5686.
(68) DiMagno, T. J.; Bylina, E. J.; Angerhofer, A.; Youvan, D. C.; Norris, J. R. *Biochemistry* **1990**, *29*, 899-.
(69) Frank, H. A.; Innes, J.; Aldema, M.; Neumann, R.; Schenck, C. C. *Photosynth. Res.* **1993**, *33*, 99-.
(70) Palaniappan, V.; Schenck, C. C.; Bocian, D. *J. Phys. Chem.* **1995**, *99*, 17049-.
(71) Allen, J. P.; Artz, K.; Lin, X.; Williams, J. C.; Ivancich, A.; Albouy, D.; Mattioli, T. A.; Fetsch, A.; Kuhn, M.; Lubitz, W. *Biochemistry* **1996**, *35*, 6612−6619.
(72) Zhou, H.; Boxer, S. G. *J. Phys. Chem. B* **1997**, *101*, 5759−5766.
(73) Davis, D.; Dong, A.; Caughey, W. S.; Schenck, C. *Biophys. J.* **1992**, *61*, A153.
(74) Laible, P. D.; Kirmaier, C.; Udawatte, C. S. M.; Hofman, S. J.; Holten, D.; Hanson, D. K. *Biochemistry* **2003**, *42*, 1718−1730.
(75) Kirmaier, C.; Laible, P. D.; Hinden, E.; Hanson, D. K.; Holten, D. *Chem. Phys.* **2003**, *294*, 305−318.
(76) Laible, P. D.; Scott, H. N.; Henry, L.; Hanson, D. K. *J. Struct. Funct. Genomics* **2004**, *5*, 167−173.
(77) Kirmaier, C.; Holten, D. *Biochemistry* **1991**, *30*, 609−613.
(78) Yang, S. I.; Li, J. Z.; Cho, H. S.; Kim, D.; Bocian, D. F.; Holten, D.; Lindsey, J. S. *J. Mater. Chem.* **2000**, *10*, 283−296.
(79) Prince, R. C.; Youvan, D. C. *Biochim. Biophys. Acta* **1987**, *890*, 286−291.
(80) Chirino, A. J.; Lous, E. J.; Huber, M.; Allen, J. P.; Schenck, C. C.; Paddock, M. L.; Feher, G.; Rees, D. C. *Biochemistry* **1994**, *33*, 4584−4593.
(81) Camara-Artigas, A.; Magee, C.; Goetsch, A.; Allen, J. P. *Photosynth. Res.* **2002**, *74*, 87−93.
(82) Kirmaier, C.; Gaul, D.; DeBey, R.; Holten, D.; Schenck, C. C. *Science* **1991**, *251*, 922−927.
(83) In wild-type RCs there is a clear spectral distinction between bleaching of the ground-state absorption of P (850-nm maximum for *R. capsulatus* in LDAO) and stimulated emission from P* (920-nm maximum). For the heterodimers, the contribution of stimulated emission to the spectra in Figure 4A and B is much more difficult to assess; however, it has been shown that the D* spontaneous fluorescence is considerably to the red of the main part of the D absorption feature, analogous to wild-type RCs. At low temperature the D* fluorescence peak is near 970 nm (King, B. A.; Stanley, R. J.; Boxer, S. G. *J. Phys. Chem. B* **1997**, *101*, 3644−3648.) Stimulated emission from the heterodimers has been resolved at wavelengths >920 nm at low temperature.[62]
(84) Previously, it was reported for the Mhd RC in *R. capsulatus* that the D* lifetime was ∼14 ps and the yield of initial L-side charge separation was 50%, with 50% decay of D* to the ground state.[56] This contrasts with 25% charge separation and 75% deactivation to the ground-state found here. We have no ready explanation for this difference; perhaps it is related to slight differences in sample preparation or the presence of the His tag on the protein in the work here.
(85) Kwa, S. L. S.; Folker, S.; Tilly, N. T.; Van Grondelle, R.; Dekker, J. P. *Photochem. Photobiol.* **1994**, *59*, 219−228.
(86) Breton, J.; Bylina, E. J.; Youvan, D. C. *Biochemistry* **1989**, *28*, 6423-.
(87) We were unable to detect electron transfer to H_M from D* in the Mhd and Lhd RCs. In principle, the value of k_M in these RCs should be the same as that obtained for Mhd-β and Lhd-β RCs, $(1000\ \text{ps})^{-1}$ and $(670\ \text{ps})^{-1}$, respectively. Using these rate constants for k_M together with the D* lifetimes for the Mhd and Lhd RCs in Table 1, we can predict the yields of electron transfer to the M side of ∼1.5% and ∼3.7% for Mhd and Lhd RCs, respectively. Such low yields are beyond our signal-to-noise to resolve in the Q_X region in the presence of $P^+H_L^-$ formed at ∼10-fold higher yield. However, $P^+H_M^-$ yields of several percent are not inconsistent with the data for the Lhd and Mhd RCs (Figure 7).